Evolution of structural distortions in solid solutions between BiMnO$_3$ and BiScO$_3$

Alexei A. Belik [a,*], Kenichi Kato [b], Eiji Takayama-Muromachi [a]

[a] International Center for Materials Nanoarchitectonics (MANA), National Institute for Materials Science (NIMS), 1-1 Namiki, Tsukuba, Ibaraki 305-0044, Japan
[b] Structural Materials Science Laboratory, RIKEN SPring-8 Center, 1-1-1 Kouto, Sayo-cho, Hyogo 679-5148, Japan

ARTICLE INFO

ABSTRACT

Crystal structures of solid solutions of BiMn$_{1-x}$Sc$_x$O$_3$ with $x = 0.05$, 0.1, 0.2, 0.3, 0.4, 0.5, and 0.7 were studied with synchrotron X-ray powder diffraction. The strong Jahn–Teller distortion, observed in BiMnO$_3$ at 300 K and associated with orbital order, disappeared already in BiMn$_{0.95}$Sc$_{0.05}$O$_3$. The orbital-ordered phase did not appear in BiMn$_{0.95}$Sc$_{0.05}$O$_3$ down to 90 K. Almost the same octahedral distortions were observed in BiMn$_{1-x}$Sc$_x$O$_3$ with $0.05 \leqslant x \leqslant 0.7$ at room temperature and in BiMnO$_3$ at 550 K above the orbital ordering temperature $T_{OO} = 473$ K. These results allowed us to conclude that the remaining octahedral distortions observed in BiMnO$_3$ above T_{OO} are the structural feature originated from the highly distorted monoclinic structure.

© 2008 Elsevier Inc. All rights reserved.

1. Introduction

BiMnO$_3$ and BiFeO$_3$ are one of the most studied multiferroic materials [1] among perovskite-type oxides. BiFeO$_3$ is the only compound among BiMO$_3$ (M = transition metals) that can be prepared at ambient pressure in bulk form. BiFeO$_3$ is an antiferromagnet and a ferroelectric material [2]. BiMnO$_3$ is the only compound among BiMO$_3$ exhibiting true ferromagnetism [1]. In addition, the orbital degrees of freedom of Mn^{3+} are active in BiMnO$_3$ resulting in the orbital-ordered state [3–6].

BiMnO$_3$ has a highly distorted perovskite-type structure at room temperature (RT) and crystallizes in a monoclinic system [3–5]. BiMnO$_3$ undergoes two high-temperature phase transitions at $T_{OO} = 474$ K and $T_{str} = 768$ K [7–9]. The phase transition at 474 K is a monoclinic-to-monoclinic phase transition accompanied by a thermal effect, abrupt changes of lattice parameters and unit cell volume, and a small jump of resistivity and magnetization [5,8,10]. Structural analysis from neutron powder diffraction data allowed us to suggest that this phase transition corresponds to orbital order (OO) below T_{OO} [5]. The phase transition at 768 K is a structural monoclinic-to-orthorhombic transition [8].

The monoclinic modification of BiMnO$_3$ which is stable below T_{OO} (space group $C2/c$) is called phase I [5,10,11]. Phase I is characterized by a monoclinic angle of about 110.6°. The monoclinic modification of BiMnO$_3$ which is stable above T_{OO}

(space group $C2/c$) is called phase II [5,10]. Phase II is characterized by a monoclinic angle of about 108.8°.

The recent first principle calculations showed that the splitting of e_g orbitals in BiMnO$_3$ at 550 K (that is, in phase II) is about 2100 K even for the Mn1 site with the smallest octahedral distortion suggesting the existence of orbital order of a different type in phase II of BiMnO$_3$ above T_{OO} [12].

In this work, we investigated structural properties of solid solutions BiMn$_{1-x}$Sc$_x$O$_3$ in attempt to understand the origin of the remaining octahedral distortions in BiMnO$_3$ above T_{OO}. We found that the rather strong octahedral distortions remain in highly diluted BiMn$_{1-x}$Sc$_x$O$_3$ samples with $x \geqslant 0.5$ where the orbital order cannot survive. The obtained results indicate that the origin of the remaining octahedral distortions is probably the structural feature of the highly distorted monoclinic structure of BiMnO$_3$.

2. Experimental

The synthesis and detailed magnetic characterization of BiMn$_{1-x}$Sc$_x$O$_3$ with specific heat and dc/ac magnetic susceptibilities are described in Refs. [13,14]. Synchrotron X-ray powder diffraction (SXRD) data of BiMn$_{1-x}$Sc$_x$O$_3$ for structure refinements were collected at RT (also at 90 K for BiMn$_{0.95}$Sc$_{0.05}$O$_3$) on a large Debye–Scherrer camera at the BL02B2 beam line of SPring-8 [15]. Incident beams from a bending magnet were monochromatized to $\lambda = 0.4227$ Å. The samples were packed in glass capillary tubes with an inner diameter of 0.2 mm, and the tubes were rotated during measurements. The SXRD data were collected in a 2θ range

from $1°$ to $50°$ with a step interval of $0.01°$. Structure parameters of $BiMnO_3$ at 550 K [5] were used as initial ones in the Rietveld refinements using RIETAN-2000 software [16]. Coefficients for analytical approximation to atomic scattering factors for Bi, Sc, Mn, and O were taken from Ref. [17]. The pseudo-Voigt function of Toraya was used as a profile function [18]. The background was represented by a composite background function, i.e., 11th-order Legendre polynomial multiplied by a set of numerical values to approximate the background. The occupancy factor, g, of all the sites was unity ($g = 1$). Isotropic atomic displacement parameters, B, with the isotropic Debye–Waller factor represented as $\exp((-B\sin^2\theta)/\lambda^2)$ were assigned to all the sites. For the impurity of $Bi_2O_2CO_3$, we refined only a scale factor and the lattice parameters, fixing its structure parameters [19]. The mass percentage of $Bi_2O_2CO_3$ was calculated from the refined scale factors to be about 1% in all the samples. In $BiMn_{0.95}Sc_{0.05}O_3$, about 5% of phase I was found [13].

3. Results and discussion

Final lattice parameters, R factors, fractional coordinates, B parameters, and some bond lengths of $BiMn_{1-x}Sc_xO_3$ are listed in Tables 1–3. Fig. 1 displays observed, calculated, and difference SXRD patterns of $BiMn_{0.8}Sc_{0.2}O_3$ as an example. Figs. 2–4 show the compositional dependence of the M–O bond lengths, distortion parameters (Δ) of MO_6 [20], $M1$–O–$M2$ bond angles ($M = $ (Mn/Sc)), and bond-valence sums [21] and Δ values for BiO_N polyhedra (calculated with $N = 8$ and 10) [20].

In the structure analyses, we assumed random distribution of Sc^{3+} ions between two crystallographically distinct sites for Mn in $BiMnO_3$. These sites are very similar to each other in size (the average bond lengths are 2.030 Å for Mn1 and 2.036 Å for Mn2 [5]). However, they are different in symmetry. The Mn2 site is located in the center of symmetry. Therefore, the O–Mn2–O bond angles with the opposite oxygen atoms are constrained to be $180°$ by the symmetry. The Mn1 site has only a twofold rotational symmetry. There is another strong argument (in addition to the site size) in favor of the random Sc^{3+} distribution. We found that the end members $BiMnO_3$ and $BiScO_3$ crystallize in space group $Pnma$ (the $GdFeO_3$-type structure) at high pressure of 4–8 GPa and RT [22]. Therefore, at the synthesis conditions at high pressure

Table 1
Structure parameters of $BiMn_{0.95}Sc_{0.05}O_3$ at 300 and 90 K.[a]

Site	Wyckoff position	x	y	z	B (Å^2)
Bi	8f	0.13409(7)	0.21411(9)	0.12841(11)	0.983(11)
		0.13439(6)	0.21318(8)	0.12874(9)	0.552(10)
$M1$	4e	0	0.2284(5)	0.75	0.90(9)
		0	0.2288(5)	0.75	0.54(7)
$M2$	4d	0.25	0.25	0.5	0.82(10)
		0.25	0.25	0.5	0.65(8)
O1	8f	0.0894(9)	0.1932(16)	0.5909(11)	1.2(2)
		0.0915(9)	0.1932(15)	0.5930(11)	0.5(2)
O2	8f	0.1659(11)	0.5565(16)	0.3897(14)	1.4(2)
		0.1666(12)	0.5579(18)	0.3903(15)	2.1(3)
O3	8f	0.3598(9)	0.5635(14)	0.1630(10)	0.8(2)
		0.3597(9)	0.5618(14)	0.1610(10)	0.6(2)

[a] Space group $C2/c$ (no. 15); $Z = 8$; $a = 9.58623(15)$ Å, $b = 5.59798(7)$ Å, $c = 9.76139(14)$ Å, $\beta = 108.8971(11)°$, and $V = 495.597(12)$ Å^3, $R_{wp} = 2.34\%$ ($S = R_{wp}/R_e = 0.98$), $R_p = 1.66\%$, $R_B = 1.24\%$, and $R_F = 1.38\%$ at 300 K and $a = 9.57404(15)$ Å, $b = 5.58899(7)$ Å, $c = 9.76023(14)$ Å, $\beta = 108.9728(10)°$, and $V = 493.889(12)$ Å^3, $R_{wp} = 2.44\%$ ($S = 1.12$), $R_p = 1.72\%$, $R_B = 1.05\%$, and $R_F = 0.91\%$ at 90 K. The occupation of all the sites is unity; $g(Mn) = 0.95$ and $g(Sc) = 0.05$ for the $M1$ and $M2$ sites. The first (x, y, z, and B) line of each site is for 300 K, the second one is for 90 K. Numbers in parentheses are statistical errors of the last significant digits.

Table 2
Selected bond lengths, l (Å), angles, ϕ (deg), and distortion parameters of MO_6 and BiO_N, Δ, in $BiMn_{0.95}Sc_{0.05}O_3$ at 90 and 300 K.

	90 K	300 K
Bi–O2	2.156(9)	2.169(9)
Bi–O3	2.203(9)	2.187(9)
Bi–O1	2.314(9)	2.327(9)
Bi–O1a	2.516(9)	2.493(9)
Bi–O2a	2.760(12)	2.763(11)
Bi–O3a	2.847(9)	2.855(9)
Bi–O3b	2.876(9)	2.883(9)
Bi–O2b	3.132(12)	3.125(11)
Bi–O1b	3.147(8)	3.178(9)
Bi–O3b	3.235(8)	3.285(8)
$\Delta(BiO_8)$	164.4×10^{-4}	164.4×10^{-4}
$\Delta(BiO_{10})$	196.4×10^{-4}	202.6×10^{-4}
$M1$–O1 ($\times 2$)	2.007(10)	2.012(11)
$M1$–O2 ($\times 2$)	2.102(13)	2.106(12)
$M1$–O3 ($\times 2$)	2.106(8)	2.112(8)
$\Delta(M1O_6)$	4.9×10^{-4}	4.9×10^{-4}
$M2$–O1 ($\times 2$)	2.031(9)	2.036(10)
$M2$–O2 ($\times 2$)	2.047(12)	2.047(11)
$M2$–O3 ($\times 2$)	1.899(9)	1.909(9)
$\Delta(M2O_6)$	11.1×10^{-4}	9.8×10^{-4}
$M1$–O1–$M2$ ($\times 2$)	154.3(5)	153.2(5)
$M1$–O2–$M2$ ($\times 2$)	154.4(5)	155.0(5)
$M1$–O3–$M2$ ($\times 2$)	151.1(5)	150.0(5)

$\Delta = (1/N)\sum_{i=1}^{N}[(l_i - l_{av})/l_{av}]^2$, where $l_{av} = (1/N)\sum_{i=1}^{N}l_i$ is the average M–O or Bi–O distance and N is the coordination number.

and high temperature, solid solutions $BiMn_{1-x}Sc_xO_3$ most probably have the $Pnma$ (or higher) symmetry with one crystallographic site for Mn^{3+} and Sc^{3+} and, therefore, random distribution of these ions. This random distribution should remain after the quenching and pressure release at RT.

Below T_{OO} in phase I, there are two long Mn–O distances in $BiMnO_3$, and octahedral distortions of MnO_6 are very large ($\Delta(Mn1O_6)*10^4 = 37.2$ and $\Delta(Mn2O_6)*10^4 = 51.3$) [5]. They are even larger than the octahedral distortion of MnO_6 in $LaMnO_3$ at RT ($\Delta(MnO_6)*10^4 = 33.1$), a classical system with orbital order [20]. Above T_{OO} in phase II, the octahedral distortions of MnO_6 are considerably reduced in $BiMnO_3$ ($\Delta(Mn1O_6)*10^4 = 4.5$ and $\Delta(Mn2O_6)*10^4 = 15.4$) [5], but the reduction is not so dramatic as that of $LaMnO_3$ above $T_{OO} = 750$ K ($\Delta(MnO_6)*10^4 = 0.9$) [20].

$BiMn_{1-x}Sc_xO_3$ with $0.05 \leqslant x \leqslant 1$ crystallizes in the phase II structure. The M–O bond lengths and Δ values in $BiMnO_3$ at 550 K and in $BiMn_{0.9}Sc_{0.1}O_3$ at RT are almost identical (Fig. 2). The same tendency is kept for the whole range of solid solutions $BiMn_{1-x}Sc_xO_3$ with $0.05 \leqslant x \leqslant 0.7$. Noticeable octahedral distortions remain especially for the $M2$ site with the center of symmetry even in $BiMn_{0.3}Sc_{0.7}O_3$. It is obvious that the orbital order cannot survive at such high-doping concentrations.

In solid solutions $LaMn_{1-x}Ga_xO_3$, the distortion of (Mn/Ga)O_6 octahedra is gradually decreased with increasing x, and samples with $x \geqslant 0.6$ show almost regular (Mn/Ga)O_6 octahedra ($\Delta((Mn/Ga)O_6)*10^4 = 0.09$ for $x = 0.6$ at 300 K) [23,24]. Another work reported a nearly regular (Mn/Ga)O_6 octahedron in La_2MnGaO_6 ($\Delta((Mn/Ga)O_6)*10^4 = 0.06$ at 300 K) [25]. In principle, the same behavior should be observed in the solid solutions $BiMn_{1-x}Sc_xO_3$. However, $BiMn_{1-x}Sc_xO_3$ crystallizes in a highly distorted perovskite structure (space group $C2/c$) in comparison with orthorhombic $LaMn_{1-x}Ga_xO_3$. Therefore, we can conclude that the origin of the remaining octahedral distortions in $BiMn_{1-x}Sc_xO_3$ is the highly distorted monoclinic structure. However, we should

Table 3
Structural parameters and R factors of $BiMn_{1-x}Sc_xO_3$ with $x = 0.1$, 0.2, 0.3, 0.4, 0.5, and 0.7 at room temperature.

x	0.1	0.2	0.3	0.4	0.5	0.7
a (Å)	9.60346(15)	9.62599(15)	9.64528(16)	9.67209(18)	9.7024(2)	9.7725(3)
b (Å)	5.61121(8)	5.63898(8)	5.66529(9)	5.69221(9)	5.71651(10)	5.76097(13)
c (Å)	9.76888(14)	9.79177(15)	9.81772(17)	9.85067(18)	9.8829(2)	9.9492(3)
β (°)	108.7682(10)	108.6032(10)	108.5073(11)	108.4441(12)	108.4159(13)	108.3884(16)
x (Bi)	0.13443(6)	0.13487(7)	0.13512(7)	0.13538(7)	0.13554(7)	0.13588(9)
y (Bi)	0.21326(8)	0.21085(9)	0.20796(9)	0.20463(9)	0.20180(12)	0.19623(12)
z (Bi)	0.12884(9)	0.12951(10)	0.13051(9)	0.13125(8)	0.13206(9)	0.13348(10)
B (Bi)	0.993(12)	1.050(13)	1.154(14)	1.196(15)	1.081(15)	1.09(2)
y (M1)	0.2272(5)	0.2274(5)	0.2310(5)	0.2319(5)	0.2343(5)	0.2407(5)
B (M1)	0.83(8)	0.81(9)	0.54(9)	0.70(9)	0.58(10)	0.05(12)
B (M2)	0.69(8)	0.89(10)	1.51(11)	1.38(11)	1.32(12)	1.88(16)
x (O1)	0.0895(8)	0.0877(9)	0.0899(9)	0.0891(8)	0.0874(8)	0.0854(10)
y (O1)	0.1891(14)	0.1904(15)	0.1922(15)	0.1898(14)	0.1935(14)	0.1984(18)
z (O1)	0.5892(9)	0.5862(10)	0.5896(10)	0.5893(9)	0.5867(9)	0.5840(11)
B (O1)	1.3(2)	1.6(2)	1.3(2)	1.4(2)	0.7(2)	0.6(3)
x (O2)	0.1617(10)	0.1621(10)	0.1680(10)	0.1664(10)	0.1648(9)	0.1643(12)
y (O2)	0.5614(14)	0.5626(14)	0.5577(15)	0.5590(15)	0.5594(14)	0.5549(19)
z (O2)	0.3824(11)	0.3740(11)	0.3753(11)	0.3745(10)	0.3735(10)	0.3720(13)
B (O2)	1.2(2)	0.7(2)	1.3(2)	1.4(2)	1.1(2)	1.2(3)
x (O3)	0.3591(8)	0.3618(9)	0.3612(9)	0.3596(9)	0.3580(9)	0.3564(11)
y (O3)	0.5591(14)	0.5503(15)	0.5433(15)	0.5389(15)	0.5416(15)	0.5375(18)
z (O3)	0.1606(9)	0.1606(10)	0.1610(9)	0.1622(9)	0.1599(9)	0.1611(12)
B (O3)	1.2(2)	1.1(2)	1.3(2)	1.4(2)	1.7(2)	1.2(3)
R_{wp}	2.54	2.51	2.23	2.99	2.68	3.53
R_p	1.79	1.73	1.63	2.16	1.90	2.53
R_B	0.84	1.00	1.42	1.69	0.62	0.96
R_F	1.10	1.29	1.43	2.02	0.62	0.85
S	1.78	1.52	1.04	1.76	1.59	2.08

See Table 1 for Wyckoff positions of the sites and other information. Mn and Sc atoms are distributed randomly between the $M1$ and $M2$ sites (that is, $g(Mn) = 1-x$ and $g(Sc) = x$).
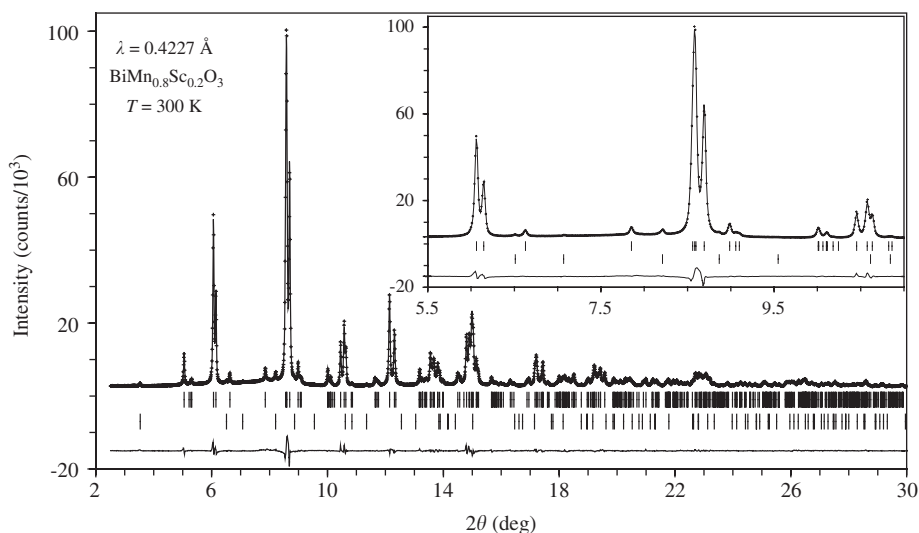

Fig. 1. Portions of observed (crosses), calculated (solid line), and difference patterns resulting from the Rietveld analysis of the synchrotron X-ray powder diffraction data of $BiMn_{0.8}Sc_{0.2}O_3$ at 300 K. Bragg reflections are indicated by tick marks. The lower tick marks are given for reflections from the impurity $Bi_2O_2CO_3$ (1.2 wt%). The inset gives the enlarged fragment.

emphasize that Sc^{3+} ions can have the second-order Jahn–Teller effect [26]. Combinations of ions with the first-order Jahn–Teller effect (Mn^{3+}) and second-order Jahn-Teller effect (Sc^{3+}) may contribute to the increase of the structural distortion. We note that the structural analysis gives an average static picture of crystal structures. To the best of our knowledge, there is no structural information (compositional dependence of M–O bond lengths) about the solid solutions $LaMn_{1-x}Sc_xO_3$. But the compositional dependence of the lattice parameters of $LaMn_{1-x}Sc_xO_3$ [27] is different from those of $LaMn_{1-x}Al_xO_3$ [27] and $LaMn_{1-x}Ga_xO_3$ [23] suggesting probably a different behavior of M–O bond

lengths. In this content, investigations of effects of non-degenerate M^{3+} ions without the second-order Jahn-Teller effect ($M = Al^{3+}$ (d^0), Cr^{3+} (d^3), Fe^{3+} (d^5), and Ga^{3+} (d^{10})) on the structural distortions of $BiMn_{1-x}M_xO_3$ may be interesting. For example, in La_2MnMO_6 with non-degenerate $M = Ga^{3+}$ [25], Cr^{3+} [28], and Fe^{3+} [28], these ions have the same effect, that is, the resulting $(Mn/M)O_6$ octahedra are almost regular ($\Delta((Mn/Ga)O_6)*10^4 = 0.06$, $\Delta((Mn/Cr)O_6)*10^4 = 0.12$, and $\Delta((Mn/Fe)O_6)*10^4 = 1.61$).

The M–O bond lengths and Δ values in $BiMn_{0.95}Sc_{0.05}O_3$ at 300 and 90 K are very similar to each other (Table 2), and $BiMn_{0.95}Sc_{0.05}O_3$ adopts the phase II structure. This fact shows
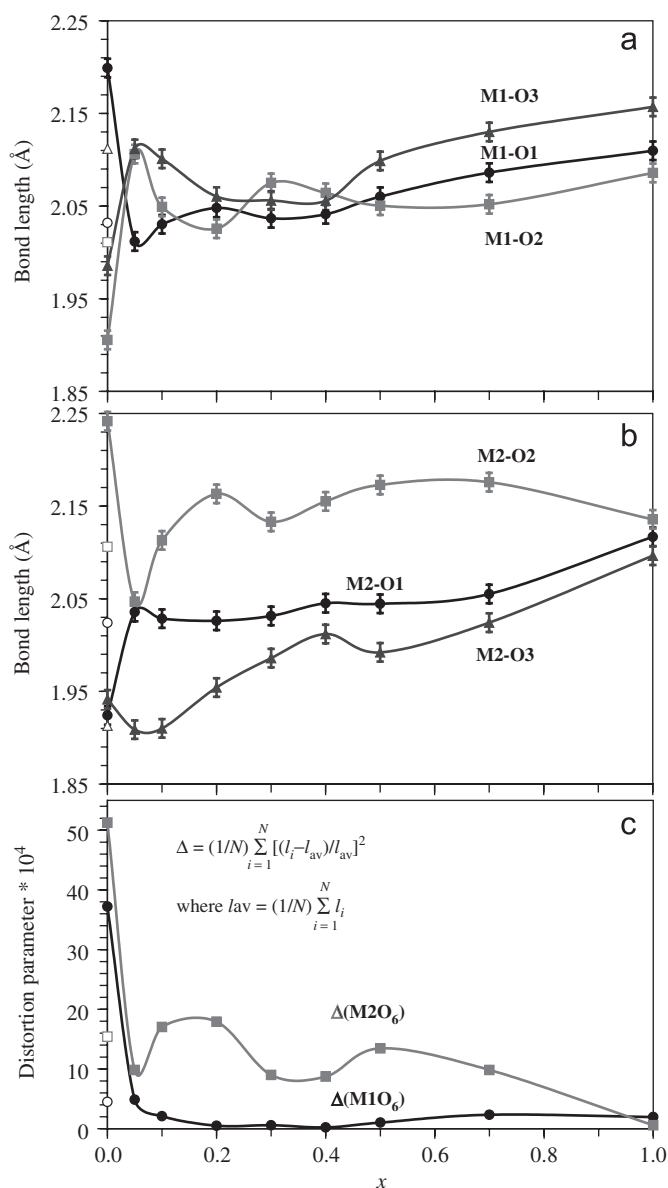
Fig. 2. Compositional dependence of (a) $M1$–O bond lengths, (b) $M2$–O bond lengths, and (c) octahedral distortion parameters $\Delta(M1O_6)$ and $\Delta(M2O_6)$ in solid solutions $BiMn_{1-x}Sc_xO_3$ at 300 K. The white symbols show the values for $BiMnO_3$ at 550 K [5]. The values for $BiScO_3$ are taken from Ref. [30].

that (1) phase II is stabilized very fast with the substitution in the Mn sublattice and (2) phase II is stable down to 90 K, and the orbital-ordered phase I does not appear.

The stability and distortions of perovskite-type oxides can be qualified using the tolerance factor, t:

$$t = \frac{r_A + r_O}{\sqrt{2}(r_B + r_O)} \tag{1}$$

where r_A, r_B, and r_O are the ionic radii of the A, B, and oxygen ions, respectively, in a perovskite ABO_3; and $t = 1$ for an ideal undistorted perovskite. With $r_{VIII}(Bi^{3+}) = 1.17$ Å, $r_{VI}(Sc^{3+}) = 0.745$ Å, $r_{VI}(Mn^{3+}) = 0.645$ Å, and $r_{VI}(O^{2-}) = 1.40$ Å [29], we have $t(BiScO_3) = 0.847$ and $t(BiMnO_3) = 0.889$. That is, $BiScO_3$ should be more distorted. This fact can be seen from the compositional change of the distortion parameter of the BiO_N polyhedra (Fig. 4) and $M1$–O–$M2$ bond lengths (Fig. 3). The $\Delta(BiO_N)$ values are almost constant for $0.0 \leqslant x \leqslant 0.2$, and then they gradually increase with increasing x in $BiMn_{1-x}Sc_xO_3$. The dispersion of the

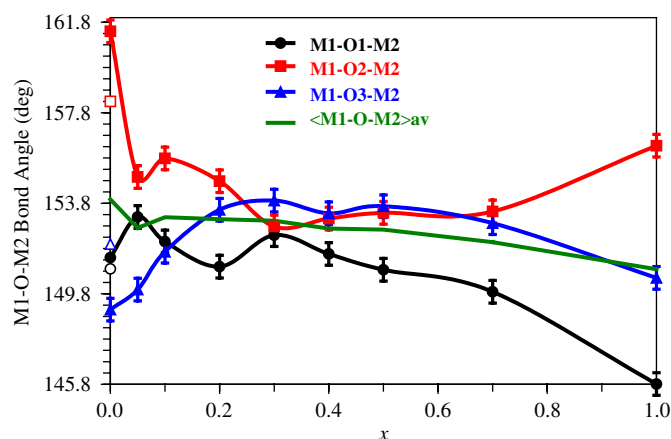**Fig. 3.** Compositional dependence of $M1$–O–$M2$ bond angles in solid solutions $BiMn_{1-x}Sc_xO_3$ at 300 K. The white symbols show the values for $BiMnO_3$ at 550 K [5]. The values for $BiScO_3$ are taken from Ref. [30].
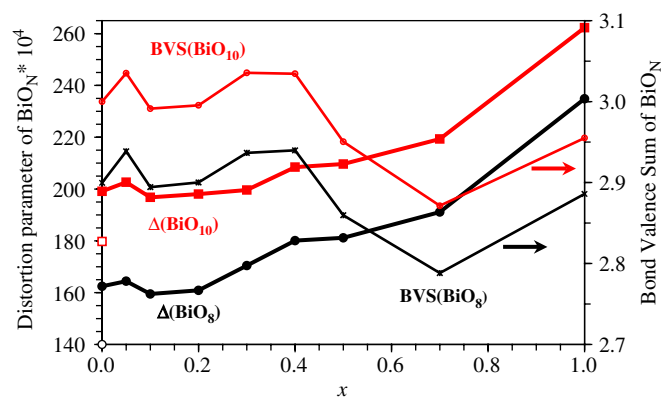

Fig. 4. Compositional dependence of bond valence sums (BVS [21]) for Bi^{3+} (right-hand scale) and distortion parameters $\Delta(BiO_N)$ with $N = 8$ and 10 (left-hand scale) in solid solutions $BiMn_{1-x}Sc_xO_3$ at 300 K. The white symbols show the values for $BiMnO_3$ at 550 K [5].

$M1$–O–$M2$ bond lengths is the largest for $BiScO_3$ compared with $BiMn_{1-x}Sc_xO_3$ ($0.05 \leqslant x \leqslant 0.7$). The large Mn1–O–Mn2 bond length dispersion in $BiMnO_3$ at RT is probably related to the large distortions of the MnO_6 octahedra due to the Jahn–Teller effect. The second-order Jahn–Teller effect of Sc^{3+} is rather weak; therefore, the distortion of the ScO_6 octahedra is small in pure $BiScO_3$ (Fig. 2c). The expected (from the tolerance factor) larger distortion of $BiScO_3$ is achieved by the larger distortion of the BiO_N polyhedra and rotation of the ScO_6 octahedra. The introduction of the Jahn–Teller active Mn^{3+} ions into $BiScO_3$ induces a noticeable distortion of the $M2$ site and reduction of the BiO_N polyhedra distortion.

In this paragraph, we would like to give some comments on the question about the origin of the highly distorted monoclinic structure of $BiMnO_3$. This question is a part of a more general problem: why crystal symmetries of $BiMnO_3$ [5] ($BiScO_3$ [30] and $BiCrO_3$ [31]), $BiFeO_3$ [2], $BiCoO_3$ [32], and $BiNiO_3$ [33] are different (at RT and ambient pressure). All these compounds have Bi^{3+} ions with a lone electron pair in the A-site of the perovskite structure. The orbital order of $BiMnO_3$ alone cannot be crucial because $BiScO_3$ and $BiCrO_3$ have the same distorted structure and no OO. Ionic radii [29] of Sc^{3+} ($r_{VI} = 0.745$ Å), Cr^{3+} ($r_{VI} = 0.615$ Å), and Mn^{3+} ($r_{VI} = 0.645$ Å) are quite different. On the other hand, ionic radii of Fe^{3+} ($r_{VI} = 0.645$ Å) and Mn^{3+} ($r_{VI} = 0.645$ Å) are the same, however, they have different distortions (space group $R3c$ for

BiFeO$_3$ and $C2/c$ for BiMnO$_3$). Ionic radii of Cr^{3+} (r_{VI} = 0.615 Å) and Co^{3+} (r_{VI} = 0.610 Å) are also close but distortions are different (space group $C2/c$ for BiCrO$_3$ and $P4mm$ for BiCoO$_3$). Therefore, simple crystal chemistry considerations cannot give the answer about the origin of different symmetries. Some ideas about the origin of the $P4mm$ symmetry of BiCoO$_3$ are given in Ref. [34]. It is interesting that many of the BiMO$_3$ compounds have the $Pnma$ symmetry at high pressure and RT [22,33] similar to LaMO$_3$ (at RT and ambient pressure). Therefore, the pressure seems to remove distortions caused by the presence of a lone electron pair of Bi^{3+}. The symmetry at ambient pressure is governed by unique properties of each transition metal coupled with the presence of a lone electron pair of Bi^{3+}.

In conclusion, the structural properties of the solid solutions BiMn$_{1-x}$Sc$_x$O$_3$ have been investigated. Almost the same octahedral distortions were observed in BiMn$_{1-x}$Sc$_x$O$_3$ with $0.05 \leqslant x \leqslant 0.7$ at RT and in BiMnO$_3$ at 550 K above the orbital ordering temperature T_{OO} = 473 K. These results allowed us to conclude that the remaining octahedral distortions observed in BiMnO$_3$ above T_{OO} are the structural feature originated from the highly distorted monoclinic structure.

Acknowledgments

References

[1] R. Ramesh, N.A. Spaldin, Nat. Mater. 6 (2007) 21.
[2] J. Wang, J.B. Neaton, H. Zheng, V. Nagarajan, S.B. Ogale, B. Liu, D. Viehland, V. Vaithyanathan, D.G. Schlom, U.V. Waghmare, N.A. Spaldin, K.M. Rabe, M. Wuttig, R. Ramesh, Science 299 (2003) 1719.
[3] T. Atou, H. Chiba, K. Ohoyama, Y. Yamaguchi, Y. Syono, J. Solid State Chem. 145 (1999) 639.
[4] A. Moreira dos Santos, A.K. Cheetham, T. Atou, Y. Syono, Y. Yamaguchi, K. Ohoyama, H. Chiba, C.N.R. Rao, Phys. Rev. B 66 (2002) 64425.
[5] A.A. Belik, S. Iikubo, T. Yokosawa, K. Kodama, N. Igawa, S. Shamoto, M. Azuma, M. Takano, K. Kimoto, Y. Matsui, E. Takayama-Muromachi, J. Am. Chem. Soc. 129 (2007) 971.
[6] C.H. Yang, J. Koo, C. Song, T.Y. Koo, K.B. Lee, Y.H. Jeong, Phys. Rev. B 73 (2006) 224112.
[7] F. Sugawara, S. Iiida, Y. Syono, S. Akimoto, J. Phys. Soc. Jpn. 25 (1968) 1553.
[8] T. Kimura, S. Kawamoto, I. Yamada, M. Azuma, M. Takano, Y. Tokura, Phys. Rev. B 67 (2003) 180401(R).
[9] A.A. Belik, E. Takayama-Muromachi, Inorg. Chem. 46 (2007) 5585.
[10] E. Montanari, G. Calestani, A. Migliori, M. Dapiaggi, F. Bolzoni, R. Cabassi, E. Gilioli, Chem. Mater. 17 (2005) 6457.
[11] T. Yokosawa, A.A. Belik, T. Asaka, K. Kimoto, E. Takayama-Muromachi, Y. Matsui, Phys. Rev. B 77 (2008) 024111.
[12] I.V. Solovyev, Z.V. Pchelkina, New J. Phys. 10 (2008) 073021.
[13] A.A. Belik, T. Yokosawa, K. Kimoto, Y. Matsui, E. Takayama-Muromachi, Chem. Mater. 19 (2007) 1679.
[14] A.A. Belik, E. Takayama-Muromachi, J. Phys. Condens. Matter 20 (2008) 025211.
[15] E. Nishibori, M. Takata, K. Kato, M. Sakata, Y. Kubota, S. Aoyagi, Y. Kuroiwa, M. Yamakata, N. Ikeda, Nucl. Instrum. Methods Phys. Res. Sect. A 467–468 (2001) 1045.
[16] F. Izumi, T. Ikeda, Mater. Sci. Forum 321–324 (2000) 198.
[17] A.J.C. Wilson, E. Prince (Eds.), International Tables for Crystallography, vol. C, second ed., Kluwer, Dordrecht, The Netherlands, 1999, pp. 572–574.
[18] H. Toraya, J. Appl. Crystallogr. 23 (1990) 485.
[19] J.D. Grice, Can. Mineral. 40 (2002) 693.
[20] J. Rodríguez-Carvajal, M. Hennion, F. Moussa, A.H. Moudden, L. Pinsard, A. Revcolevschi, Phys. Rev. B 57 (1998) 3189(R).
[21] R.E. Brese, M. O'Keeffe, Acta Crystallogr. Sect. B 47 (1991) 192.
[22] A.A. Belik, H. Yusa, N. Hirao, Y. Ohishi, E. Takayama-Muromachi, Inorg. Chem., 2009, in press, doi:10.1021/ic8015996.
[23] J. Blasco, J. Garcia, J. Campo, M.C. Sanchez, G. Subias, Phys. Rev. B 66 (2002) 174431.
[24] M.C. Sanchez, G. Subias, J. Garcia, J. Blasco, Phys. Rev. B 69 (2004) 184415.
[25] E.J. Cussen, M.J. Rosseinsky, P.D. Battle, J.C. Burley, L.E. Spring, J.F. Vente, S.J. Blundell, A.I. Coldea, J. Singleton, J. Am. Chem. Soc. 123 (2001) 1111.
[26] P.S. Halasyamani, K.R. Poeppelmeier, Chem. Mater. 10 (1998) 2753.
[27] J.B. Goodenough, R.I. Dass, J. Zhou, Solid State Sci. 4 (2002) 297.
[28] D.V. Karpinsky, I.O. Troyanchuk, V.V. Sikolenko, J. Phys. Condens. Matter 19 (2007) 036220.
[29] R.D. Shannon, Acta Crystallogr. Sect. A 32 (1976) 751.
[30] A.A. Belik, S. Iikubo, K. Kodama, N. Igawa, S. Shamoto, M. Maie, T. Nagai, Y. Matsui, S.Yu. Stefanovich, B.I. Lazoryak, E. Takayama-Muromachi, J. Am. Chem. Soc. 128 (2006) 706.
[31] A.A. Belik, S. Iikubo, K. Kodama, N. Igawa, S. Shamoto, E. Takayama-Muromachi, Chem. Mater. 20 (2008) 3765.
[32] A.A. Belik, S. Iikubo, K. Kodama, N. Igawa, S. Shamoto, S. Niitaka, M. Azuma, Y. Shimakawa, M. Takano, F. Izumi, E. Takayama-Muromachi, Chem. Mater. 18 (2006) 798.
[33] M. Azuma, S. Carlsson, J. Rodgers, M.G. Tucker, M. Tsujimoto, S. Ishiwata, S. Isoda, Y. Shimakawa, M. Takano, J.P. Attfield, J. Am. Chem. Soc. 129 (2007) 14433.
[34] K. Oka, I. Yamada, M. Azuma, S. Takeshita, K.H. Satoh, A. Koda, R. Kadono, M. Takano, Y. Shimakawa, Inorg. Chem. 47 (2008) 7355.